INTERNATIONAL JOURNAL OF NUMERICAL MODELLING : ELECTRONIC NETWORKS, DEVICES AND FIELDS,
Vol. 10, 153–167 (1997)

GENERALIZED MODAL SCATTERING MATRIX OF DISCONTINUITY-DISTORTED WAVEGUIDE MULTIPORT JUNCTIONS

VLADIMIR A. LABAY AND JENS BORNEMANN*

Laboratory for Lightwave Electronics, Microwaves and Communications (LLiMiC), Department of Electrical and Computer Engineering, University of Victoria, Victoria B.C., Canada V8W 3P6

SUMMARY

A generalized modal scattering matrix formulation is presented for the calculation of discontinuity-distorted waveguide multiport junctions. Unlike common approaches based on three-plane mode-matching techniques, and modifications thereof, which calculate only the fundamental-mode scattering matrix, this algorithm computes the generalized modal scattering matrix of the junction. Therefore, the method allows the computation of components in which other structures are connected as closely as possible to the discontinuity-distorted junction as follows directly from the rigorous incorporation of all higher-order mode interactions. The method is demonstrated at three selected examples: the waveguide corner, the T-junction power divider and the orthomode transducer. Comparison with results obtained by other numerical techniques or measurements available from the literature are found to be in good agreement. © 1997 by John Wiley & Sons, Ltd.

Int. J. Numer. Model., **10**, 153–167 (1997)

No. of Figures: 6. No. of Tables: 0. No. of References: 20.

1. INTRODUCTION

Modern antenna feed systems for satellite applications frequently require connections of several rectangular waveguides at a certain location. The principal tasks associated with such multiport junctions include power division and multiplexing,[1–4] beamforming,[5] and polarization discrimination.[6–8] The theoretical analysis is mostly concerned with, first, deriving the scattering matrix of the junction and, second, connecting scattering matrices of other components to individual branches in order to obtain the performance of an entire (sub)system.

Computer-aided design procedures have adopted two fundamental approaches to model multiple waveguide junctions:

1. As long as the so-called resonator region — formed by the connection of at least two waveguides at right-angles — is homogeneous, i.e. it can be represented by a well-known set of cavity functions, a resonator model[9] can be applied to yield the generalized modal scattering matrix of the junction. This has been demonstrated in publications involving waveguide corners, e.g. Reference 9, numerous papers on *E*- or *H*-plane T-junctions, of which only References 1 and 2 are representatively referenced here, and a contribution on the six-port cross-junction.[10]
2. The second approach is solely based on the analysis of two-ports, e.g. Reference 11. Branching ports are initially represented by shorts some distance away from the junction. A number of theoretical experiments (e.g. three for a T-junction) with varying locations of the shorting planes provide sufficient knowledge to extract the scattering parameters of the multiport junction under investigation.[3–5]

The advantage of this second method resides in the fact that it allows discontinuities in the

* Correspondence to: Jens Bornemann, Department of Electrical and Computer Engineering, University of Victoria, PO Box 3055, Victoria, BC, Canada V8W 3P6.

CCC 0894–3370/97/030153–15$17.50

Received 22 March 1996
Revised 15 July 1996

resonator region to be incorporated in a straightforward fashion since the fundamental algorithm evaluates two-port discontinuities only. However, although these two-port discontinuities are analysed for their generalized scattering matrices, some submatrices of the generalized multiport junction will always depend *non-linearily* on those of the two-ports. (In the case of a T-junction, the dependence is given by a square-root function.) Since the resulting non-linear matrix equation system cannot, in general, be solved for the complete set of submatrices, only the fundamental-mode scattering matrix of the entire multiport junction can be extracted. This is explicitly pointed out in Reference 5: 'These [shorting] planes are located far enough so as not to perturb the reactive fields in the proximity of the discontinuity.' Therefore, if following circuitry is connected at a smaller distance, which is necessary in orthomode transducers or compact multiplexer designs, e.g. Reference 12, or, in other words, if higher-order modes *do* interact and perturb the reactive fields in the proximity of the discontinuity, then this analysis — frequently referred to as three-plane mode matching — is invalid. Recent publications on this theory[13,14] are essentially modifications of References 3–5 and 11. (It should be pointed out, however, that the authors of Reference 5 subsequently solved similar waveguide junctions based on a generalized multiport description, e.g. References 18–20.)

Therefore, this paper focuses on the presentation of the generalized modal scattering matrix for mode-matching problems involving discontinuity-distorted multiport junctions. Alternatively, the short-circuit admittance matrix[15] or the open-circuit impedance matrix, e.g. Reference 6 could be derived with essentially the same principles as applied here. These two approaches are considered advantageous with respect to computation time but lead to some numerical complications for extremely short subsections (both admittance and impedance matrices do not exist for zero-length discontinuities[15] and for a very high number of modes as required, e.g. in elliptic-function-type filter and multiplexer arrangements.[17]

Since such problems cannot occur in the more general — but admittedly more CPU-time intensive — scattering-matrix formulation, we will focus on exactly this procedure. It allows the entire generalized scattering matrix of a discontinuity-distorted multiport waveguide junction to be calculated without restrictions for connected components. Based on the rigorous field-theory treatment of discontinuities within the resonator region, a complete set of matching conditions at the junction's interfaces is derived. Consequently, higher-order mode interactions are not only considered in the calculation but are, equally importantly, appropriately represented at the multiport junction interfaces, thus allowing computation and inclusion of other components connected at zero distance to the junction.

While, in the following, the theoretical treatment will be demonstrated at the example of a discontinuity-distorted T-junction, the extension of this technique to applications involving, for example, a discontinuity-distorted six-port cross-junction is straightforward. In this paper, results are presented for waveguide corners, T-junction power dividers and orthomode transducers — all of which with some discontinuities within the junction region. Good agreement with results obtained by other numerical techniques or measurements is observed. Although theory and examples focus exclusively on cases of two-dimensional distortions within the junction region, the principal formulation for the general three-dimensional case is addressed at the end of Section 2.

2. THEORY

Figure 1 shows the discontinuity-distorted T-junction with an additional double-plane step in the interface of the branching waveguide. To formulate the electromagnetic field representation of the junction, the configuration is first subdivided into the three cross-sectional regions I, II and III and the discontinuity-distorted resonator region IV (Figure 2a). The expressions for the tangential field components in the connected waveguides I to III are:

$$\vec{\mathbf{E}}_T^{\,\mathrm{I}} = [\vec{\mathbf{e}}_T^{\,e\mathrm{I}} | \vec{\mathbf{e}}_T^{\,m\mathrm{I}}] \cdot \mathrm{diag}\,\{\sqrt{Z_{p,q}^{e,m\mathrm{I}}}\} \cdot [\mathrm{diag}\,\{\exp[-jk_{zp,q}^{e,m\mathrm{I}} z]\}\,\mathbf{A}^{\mathrm{I}} + \mathrm{diag}\,\{\exp[jk_{zp,q}^{e,m\mathrm{I}} z]\}\,\mathbf{B}^{\mathrm{I}}]$$

$$\vec{\mathbf{H}}_T^{\,\mathrm{I}} = [\vec{\mathbf{h}}_T^{\,e\mathrm{I}} | \vec{\mathbf{h}}_T^{\,m\mathrm{I}}] \cdot \mathrm{diag}\,\{\sqrt{Y_{p,q}^{e,m\mathrm{I}}}\} \cdot [\mathrm{diag}\,\{\exp[-jk_{zp,q}^{e,m\mathrm{I}} z]\}\,\mathbf{A}^{\mathrm{I}} - \mathrm{diag}\,\{\exp[jk_{zp,q}^{e,m\mathrm{I}} z]\}\,\mathbf{B}^{\mathrm{I}}] \quad (1)$$

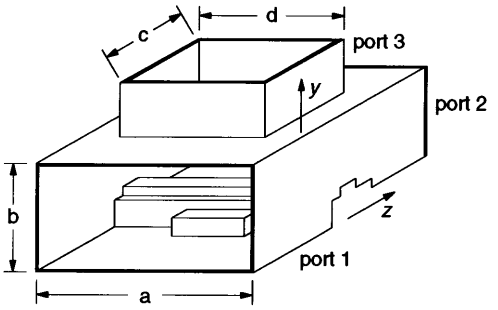

Figure 1. Rectangular-waveguide T-junction with discontinuity-distorted junction region and double-plane step in the interface of the branching waveguide

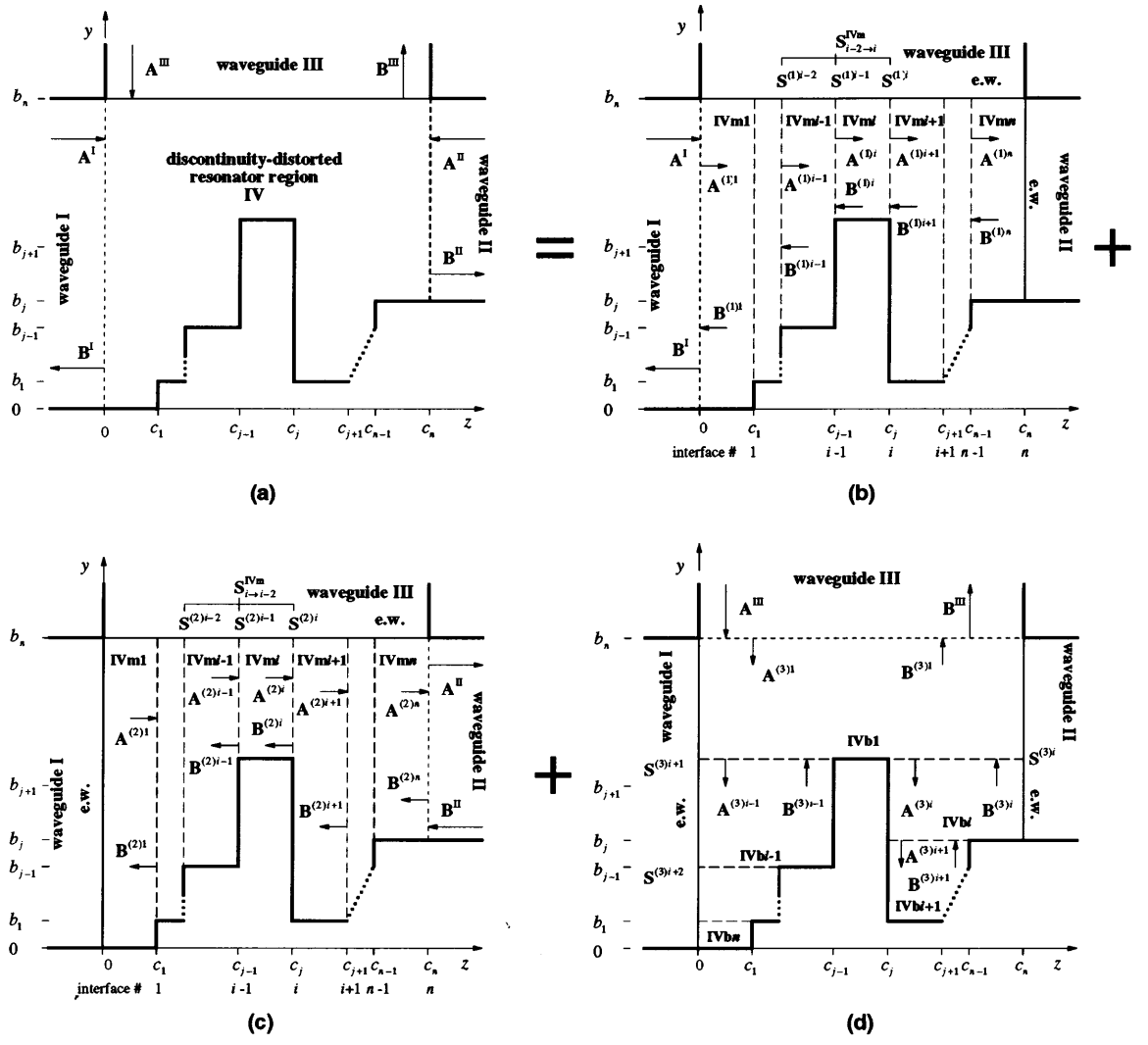

Figure 2. Superposition principle for field-theory treatment and subdivisions of resonator region: (a) T-junction with discontinuities; (b) subdivisions to match port I; (c) subdivisions to match port II; (d) subdivisions to match port III

$$\vec{\mathbf{E}}_T^{\,\mathrm{II}} = [\vec{\mathbf{e}}_T^{\,e\mathrm{II}} | \vec{\mathbf{e}}_T^{\,m\mathrm{II}}] \cdot \mathrm{diag}\,\{\sqrt{Z_{p,q}^{e,m\mathrm{II}}}\} \cdot$$
$$[\mathrm{diag}\,\{\exp[-jk_{zp,q}^{e,m\mathrm{II}}(z-c_n)]\}\,\mathbf{B}^{\mathrm{II}} + \mathrm{diag}\,\{\exp[jk_{zp,q}^{e,m\mathrm{II}}(z-c_n)]\}\,\mathbf{A}^{\mathrm{II}}]$$

$$\vec{\mathbf{H}}_T^{\,\mathrm{II}} = [\vec{\mathbf{h}}_T^{\,e\mathrm{II}} | \vec{\mathbf{h}}_T^{\,m\mathrm{II}}] \cdot \mathrm{diag}\,\{\sqrt{Y_{p,q}^{e,m\mathrm{II}}}\} \cdot$$
$$[\mathrm{diag}\,\{\exp[-jk_{zp,q}^{e,m\mathrm{II}}(z-c_n)]\}\,\mathbf{B}^{\mathrm{II}} - \mathrm{diag}\,\{\exp[jk_{zp,q}^{e,m\mathrm{II}}(z-c_n)]\}\,\mathbf{A}^{\mathrm{II}}] \quad (2)$$

$$\overrightarrow{\mathbf{E}}_T^{\mathrm{III}} = [\overrightarrow{\mathbf{e}}_T^{e\mathrm{III}} | \overrightarrow{\mathbf{e}}_T^{m\mathrm{III}}] \cdot \mathrm{diag}\,\{\sqrt{Z_{p,q}^{e,m\mathrm{III}}}\} \cdot$$
$$[\mathrm{diag}\,\{\exp[-jk_{yp,q}^{e,m\mathrm{III}}(y-b_n)]\}\,\mathbf{B}^{\mathrm{III}} + \mathrm{diag}\,\{\exp[jk_{yp,q}^{e,m\mathrm{III}}(y-b_n)]\}\,A^{\mathrm{III}}]$$

$$\overrightarrow{\mathbf{H}}_T^{\mathrm{III}} = [\overrightarrow{\mathbf{h}}_T^{e\mathrm{III}} | \overrightarrow{\mathbf{h}}_T^{m\mathrm{III}}] \cdot \mathrm{diag}\,\{\sqrt{Y_{p,q}^{e,m\mathrm{III}}}\} \cdot$$
$$[\mathrm{diag}\,\{\exp[-jk_{yp,q}^{e,m\mathrm{III}}(y-b_n)]\}\,\mathbf{B}^{\mathrm{III}} - \mathrm{diag}\,\{\exp[jk_{yp,q}^{e,m\mathrm{III}}(y-b_n)]\}\,\mathbf{A}^{\mathrm{III}}] \quad (3)$$

with well-known cross-section eigenvectors $\overrightarrow{\mathbf{e}}_T^{e,m}$, $\overrightarrow{\mathbf{h}}_T^{e,m}$, wave impedances $Z_{p,q}^{e,m} = 1/Y_{p,q}^{e,m}$ and propagation constants $k_{zp,q}^{e,m}$, $k_{yp,q}^{e,m}$. In the discontinuity-distorted resonator region IV, the electromagnetic field is determined by three solutions IV(1), IV(2) and IV(3), corresponding to individual boundary conditions (Figure 2). These regions IV are appropriately subdivided into two sets of subregions. The first set, applicable to IV(1) and IV(2), is a subdivision of region IV having all subregion interfaces perpendicular to the z-axis and the second set, pertaining to IV(3), having the subregion interfaces perpendicular to the y-axis. These subregions are labelled IVm1, IVm2, …, IVmn, and IVb1, IVb2, …, IVbn, respectively, where n is the total number of subregions in each direction (cf. Figures 2(b), (c), (d)). Note that the individual solutions to subregions IV(1), IV(2) and IV(3) correspond to short-circuit boundaries at the interfaces of the respective other two ports. This would be identical in an admittance matrix formulation. Alternatively, we could impose open-circuit boundary conditions — as required for an impedance matrix algorithm — and adjust the field representations for subregions IV(1), IV(2) and IV(3) within the junction region accordingly.

At this point, it is essential to note that the subregions IVm1, IVmn and IVb1 must have the same cross-section dimensions as waveguides I, II and III, respectively. Although this requirement applies universally, it is equally important to note that there is no loss of generality because of it. Furthermore, Figure 2 shows no variation along the x-axis even though this formulation will accommodate such a variation. Both of these situations are addressed at the end of this Section.

Starting with region IV(1) as detailed in Figure 2(b), the tangential electromagnetic fields in each region IVmi are written as

$$\overrightarrow{\mathbf{E}}_T^{\mathrm{IVm}i} = [\overrightarrow{\mathbf{e}}_T^{e\mathrm{IVm}i} | \overrightarrow{\mathbf{e}}_T^{m\mathrm{IVm}i}] \cdot \mathrm{diag}\,\{\sqrt{Z_{p,q}^{e,m\mathrm{IVm}i}}\} \cdot$$
$$[\mathrm{diag}\,\{\exp[-jk_{zp,q}^{e,m\mathrm{IVm}i}(z-c_{j-1})]\}\,\mathbf{A}^{(1)i} + \mathrm{diag}\,\{\exp[jk_{zp,q}^{e,m\mathrm{IVm}i}(z-c_{j-1})]\}\,\mathbf{B}^{(1)i}]$$

$$\overrightarrow{\mathbf{H}}_T^{\mathrm{IVm}i} = [\overrightarrow{\mathbf{h}}_T^{e\mathrm{IVm}i} | \overrightarrow{\mathbf{h}}_T^{m\mathrm{IVm}i}] \cdot \mathrm{diag}\,\{\sqrt{Z_{p,q}^{e,m\mathrm{IVm}i}}\} \cdot$$
$$[\mathrm{diag}\,\{\exp[-jk_{zp,q}^{e,m\mathrm{IVm}i}(z-c_{j-1})]\}\,\mathbf{A}^{(1)i} - \mathrm{diag}\,\{\exp[jk_{zp,q}^{e,m\mathrm{IVm}i}(z-c_{j-1})]\}\,\mathbf{B}^{(1)i}] \quad (4)$$

The tangential electric and magnetic fields are matched at the common interfaces $z = c_j$ for j = 1, 2, 3, …, n–1 between the subregions to yield the generalized scattering matrix at each interface. These scattering matrices are cascaded, *along with the homogeneous empty waveguide sections between them*, to yield a scattering matrix from any z-co-ordinate plane to another in region IV(1). Now, with a short circuit at $z = c_n$, a reflection coefficient may be defined at each interface $z = c_j$ for j = 1, 2, 3, …, n–1 by

$$\Gamma_{i-1}^{(1)} = \mathbf{S}_{11i-1\to n}^{\mathrm{IVm}} - \mathbf{S}_{12i-1\to n}^{\mathrm{IVm}}\,[\mathbf{I} + \mathbf{S}_{22i-1\to n}^{\mathrm{IVm}}]^{-1}\,\mathbf{S}_{21i-1\to n}^{\mathrm{IVm}} \quad (5)$$

Using this modal reflection coefficient and introducing transfer matrices $\mathbf{T}_{Ai-1}^{(1)}$ and $\mathbf{T}_{Bi-1}^{(1)}$, the wave amplitudes in each subregion may be expressed in terms of those of subregion IVm1. That is, the wave amplitudes $\mathbf{A}^{(1)i}$ and $\mathbf{B}^{(1)i}$ in the ith region are related to the wave amplitude $\mathbf{A}^{(1)1}$ in region IVm1 by

$$\mathbf{A}^{(1)i} = [\mathbf{I} - \mathbf{S}_{220\to i-1}^{\mathrm{IVm}}\Gamma_{i-1}^{(1)}]\mathbf{S}_{210\to i-1}^{\mathrm{IVm}}\mathbf{A}^{(1)1} = \mathbf{T}_{\mathrm{A}i-1}^{(1)}\mathbf{A}^{(1)1} \quad (6)$$

$$\mathbf{B}^{(1)i} = \Gamma_{i-1}^{(1)}\mathbf{A}^{(1)i} = \Gamma_{i-1}^{(1)}\mathbf{T}_{\mathrm{A}i-1}^{(1)}\mathbf{A}^{(1)1} = \mathbf{T}_{\mathrm{B}i-1}^{(1)}\mathbf{A}^{(1)1} \quad (7)$$

Since the subdivisions for IV(1) (Figure 2(b)) and IV(2) (Figure 2(c)) are identical, the scattering

matrices (5)–(7) at each interface $z = c_j$ for $j = 1, 2, 3, \ldots, n-1$ may be applied to IV(2) by switching the appropriate submatrices. The scattering matrix between subregions IVmi+1 and IVmi as seen in Figures 2(b), (c) is

$$\begin{bmatrix} \mathbf{A}^{(2)i+1} \\ \mathbf{B}^{(2)i} \end{bmatrix} = \begin{bmatrix} \mathbf{S}_{22}^{(1)i} & \mathbf{S}_{21}^{(1)i} \\ \mathbf{S}_{12}^{(1)i} & \mathbf{S}_{11}^{(1)i} \end{bmatrix} \begin{bmatrix} \mathbf{B}^{(2)i+1} \\ \mathbf{A}^{(2)i} \end{bmatrix} = \begin{bmatrix} \mathbf{S}_{11}^{(2)i} & \mathbf{S}_{12}^{(2)i} \\ \mathbf{S}_{21}^{(2)i} & \mathbf{S}_{22}^{(2)i} \end{bmatrix} \begin{bmatrix} \mathbf{B}^{(2)i+1} \\ \mathbf{A}^{(2)i} \end{bmatrix} \text{ at } z = c_j \tag{8}$$

Applying the boundary condition at $z = 0$, a modal reflection coefficient and transfer matrices may once again be defined at the interfaces

$$\Gamma_i^{(2)} = \mathbf{S}_{11i\to 0}^{\mathrm{IVm}} - \mathbf{S}_{12i\to 0}^{\mathrm{IVm}} \left[\mathbf{I} + \mathbf{S}_{22i\to 0}^{\mathrm{IVm}}\right]^{-1} \mathbf{S}_{21i\to 0}^{\mathrm{IVm}} \tag{9}$$

$$\mathbf{B}^{(2)i} = \left[\mathbf{I} - \mathbf{S}_{22i\to 0}^{\mathrm{IVm}} \Gamma_i^{(2)}\right] \mathbf{S}_{21i\to 0}^{\mathrm{IVm}} \mathbf{B}^{(2)n} = \mathbf{T}_{\mathrm{B}i}^{(2)} \mathbf{B}^{(2)n}$$

$$\mathbf{A}^{(2)i} = \Gamma_{i-1}^{(2)} \mathbf{B}^{(2)i} = \Gamma_{i-1}^{(2)} \mathbf{T}_{\mathrm{B}i-1}^{(2)} \mathbf{B}^{(2)n} = \Gamma_{\mathrm{A}i-1}^{(2)} \mathbf{B}^{(2)n} \tag{10}$$

so that all the amplitude coefficients for IV(2) (Figure 2(c)) can be expressed in a single unknown amplitude coefficient $\mathbf{B}^{(2)n}$ in region IVmn.

Finally, region IV(3) is subdivided according to Figure 2(d), and the tangential fields for each subregion are written as

$$\vec{\mathbf{E}}_T^{\mathrm{IVb}i} = \left[\vec{\mathbf{e}}_T^{e\mathrm{IVb}i} \middle| \vec{\mathbf{e}}_T^{m\mathrm{IVb}i}\right] \cdot \mathrm{diag}\left\{\sqrt{Z_{p,q}^{e,m\mathrm{IVb}i}}\right\} \cdot$$

$$\left[\mathrm{diag}\left\{\exp\left[-jk_{yp,q}^{e,m\mathrm{IVb}i}\,(y - b_{n-i+1})\right]\right\} \mathbf{B}^{(3)i} + \mathrm{diag}\left\{\exp\left[jk_{yp,q}^{e,m\mathrm{IVb}i}\,(y - b_{n-i+1})\right]\right\} \mathbf{A}^{(3)i}\right]$$

$$\vec{\mathbf{H}}_T^{\mathrm{IVb}i} = \left[\vec{\mathbf{h}}_T^{e\mathrm{IVb}i} \middle| \vec{\mathbf{h}}_T^{m\mathrm{IVb}i}\right] \cdot \mathrm{diag}\left\{\sqrt{Y_{p,q}^{e,m\mathrm{IVb}i}}\right\} \cdot$$

$$\left[\mathrm{diag}\left\{\exp\left[-jk_{yp,q}^{e,m\mathrm{IVb}i}\,(y - b_{n-i+1})\right]\right\} \mathbf{B}^{(3)i} - \mathrm{diag}\left\{\exp\left[jk_{yp,q}^{e,m\mathrm{IVb}i}\,(y - b_{n-i+1})\right]\right\} \mathbf{A}^{(3)i}\right] \tag{11}$$

Again, the fields are matched at the common interfaces to yield the generalized scattering matrices, and an overall scattering matrix between any two y-co-ordinate planes in region IV(3) may be calculated. With the boundary condition $\mathbf{B}^{(3)n} = -\mathbf{A}^{(3)n}$ at $y = 0$, a reflection coefficient and transfer matrices may be defined for each subregion interface, and all amplitude coefficients in region IV(3) may be written in terms of the single unknown coefficient $\mathbf{A}^{(3)1}$,

$$\Gamma_{n-i+1}^{(3)} = \mathbf{S}_{11n-i+1\to 0}^{\mathrm{IVb}} - \mathbf{S}_{12n-i+1\to 0}^{\mathrm{IVb}} \left[\mathbf{I} + \mathbf{S}_{22n-i+1\to 0}^{\mathrm{IVb}}\right]^{-1} \mathbf{S}_{21n-i+1\to 0}^{\mathrm{IVb}} \tag{12}$$

$$\mathbf{A}^{(3)i} = \left[\mathbf{I} - \mathbf{S}_{22n\to n-i+1}^{\mathrm{IVb}} \Gamma_{n-i+1}^{(3)}\right] \mathbf{S}_{21n\to n-i+1}^{\mathrm{IVb}} \mathbf{A}^{(3)1} = \mathbf{T}_{\mathrm{A}n-i+1}^{(3)} \mathbf{A}^{(3)1}$$

$$\mathbf{B}^{(3)i} = \Gamma_{n-i+1}^{(3)} \mathbf{A}^{(3)i} = \Gamma_{n-i+1}^{(3)} \mathbf{T}_{\mathrm{A}n-i+1}^{(3)} \mathbf{A}^{(3)1} = \mathbf{T}_{\mathrm{B}n-i+1}^{(3)1} \mathbf{A}^{(3)1} \tag{13}$$

In summary, all fields within the resonator region can now be expressed in terms of three still unknown coefficients in the subregions adjacent to waveguides I, II and III,

$$\vec{\mathbf{E}}^{\mathrm{IV}}(x, y, z) = \sum_{i=1}^{n} \left[\vec{\mathbf{E}}^{(1)i} + \vec{\mathbf{E}}^{(2)i} + \vec{\mathbf{E}}^{(3)i}\right] \tag{14}$$

with

$$\vec{\mathbf{E}}^{(1)i} = \left\{\left[\vec{\mathbf{e}}_T^{e\mathrm{IVm}i} \middle| \vec{\mathbf{e}}_T^{m\mathrm{IVm}i} + e_z^{m\mathrm{IVm}i} \hat{\mathbf{u}}_z\right] \mathrm{diag}\left[\sqrt{Z_{p,q}^{e,m\mathrm{IVm}i}} \exp\left[-jk_{zp,q}^{e,m\mathrm{IVm}i}\,(z - c_{i-1})\right]\right] \mathbf{T}_{\mathrm{A}i-1}^{(1)}\right.$$

$$\left. + \left[\vec{\mathbf{e}}_T^{e\mathrm{IVm}i} \middle| \vec{\mathbf{e}}_T^{m\mathrm{IVm}i} - e_z^{m\mathrm{IVm}i} \hat{\mathbf{u}}_z\right] \mathrm{diag}\left[\sqrt{Z_{p,q}^{e,m\mathrm{IVm}i}} \exp\left[jk_{zp,q}^{e,m\mathrm{IVm}i}\,(z - c_{i-1})\right]\right] \mathbf{T}_{\mathrm{B}i-1}^{(1)}\right\} \mathbf{A}^{(1)1}$$

$$\vec{\mathbf{E}}^{(2)i} = \left\{\left[\vec{\mathbf{e}}_T^{\mathrm{IVm}i} \middle| \vec{\mathbf{e}}_T^{m\mathrm{IVm}i} + e_z^{m\mathrm{IVm}i} \hat{\mathbf{u}}_z\right] \mathrm{diag}\left[\sqrt{Z_{p,q}^{e,m\mathrm{IVm}i}} \exp\left[-jk_{zp,q}^{e,m\mathrm{IVm}i}\,(z - c_i)\right]\right] \mathbf{T}_{\mathrm{A}i}^{(2)}\right.$$

$$+ [\vec{\mathbf{e}}_T^{\,e\mathrm{IVm}i} | \vec{\mathbf{e}}_T^{\,m\mathrm{IVm}i} - e_z^{m\mathrm{IVm}i}\,\hat{\mathbf{u}}_z] \operatorname{diag}[\sqrt{Z_{p,q}^{e,m\mathrm{IVm}i}} \exp[jk_{zp,q}^{e,m\mathrm{IVm}i}(z - c_i)]]\mathbf{T}_{\mathrm{B}i}^{(2)}\}\mathbf{B}^{(2)n}$$

$$\vec{\mathbf{E}}^{(3)i} = \{[\vec{\mathbf{e}}_T^{\,e\mathrm{IVb}i} | \vec{\mathbf{e}}_T^{\,m\mathrm{IVb}i} + e_y^{m\mathrm{IVb}i}\hat{\mathbf{u}}_y] \operatorname{diag}[\sqrt{Z_{p,q}^{e,m\mathrm{IVb}i}} \exp[-jk_{yp,q}^{e,m\mathrm{IVb}i}(y - b_{n-i+1})]]\mathbf{T}_{\mathrm{B}n-i+1}^{(3)}$$

$$+ [\vec{\mathbf{e}}_T^{\,e\mathrm{IVb}i} | \vec{\mathbf{e}}_T^{\,m\mathrm{IVb}i} - e_y^{m\mathrm{IVb}i}\,\hat{\mathbf{u}}_y] \operatorname{diag}[\sqrt{Z_{p,q}^{e,m\mathrm{IVb}i}} \exp[jk_{yp,q}^{e,m\mathrm{IVb}i}(y - b_{n-i+1})]]\mathbf{T}_{\mathrm{A}n-i+1}^{(3)}\}\mathbf{A}^{(3)1} \quad (15)$$

where the appropriate longitudinal terms have been added as they represent transverse components with respect to the branching waveguides.

The field continuity condition at z = 0 for the tangential electric field is

$$\vec{\mathbf{E}}_{x,y}^{\,\mathrm{I}} = \vec{\mathbf{E}}_{x,y}^{\,\mathrm{IV}} = \sum_{i=1}^{n} [\vec{\mathbf{E}}_{x,y}^{(1)i} + \vec{\mathbf{E}}_{x,y}^{(2)i} + \vec{\mathbf{E}}_{x,y}^{(3)i}] = \vec{\mathbf{E}}_{x,y}^{(1)1} \quad (16)$$

It is important to observe that, as a consequence of the choice of solutions IV(1), IV(2) and IV(3), only one single term remains in the summation over the subregions. This is consistent with mode-matching formulations for the homogeneous T-junction, e.g. References 1, 2 and 12. Applying the matching equation for the electric fields in (1), (15), as well as orthogonality and integrating over the interface area yields the relationship between the amplitude coefficients in waveguide I and the resonator region

$$\mathbf{A}^{(1)1} = [\mathbf{I} + \Gamma^{\mathrm{I}}]^{-1}\,[\mathbf{A}^{\mathrm{I}} + \mathbf{B}^{\mathrm{I}}] \quad (17)$$

Similarly, equating the electric fields at $z = c_n$ and $y = b_n$

$$\vec{\mathbf{E}}_{x,y}^{\,\mathrm{II}} = \vec{\mathbf{E}}_{x,y}^{(2)n} \text{ and } \vec{\mathbf{E}}_{x,z}^{\,\mathrm{III}} = \vec{\mathbf{E}}_{x,z}^{(3)1} \quad (18)$$

results in

$$\mathbf{B}^{(2)n} = [\mathbf{I} + \Gamma^{\mathrm{II}}]^{-1}\,[\mathbf{A}^{\mathrm{II}} + \mathbf{B}^{\mathrm{II}}]$$
$$\mathbf{A}^{(3)1} = [\mathbf{I} + \Gamma^{\mathrm{III}}]^{-1}\,[\mathbf{A}^{\mathrm{III}} + \mathbf{B}^{\mathrm{III}}] \quad (19)$$

and completes the matching procedure for the electric fields at the three junction interfaces.

Using (17) and (19), the magnetic fields in the resonator region may be completely expressed in terms of the amplitude coefficients in waveguides I, II, and III,

$$\vec{\mathbf{H}}^{\mathrm{IV}}(x, y, z) = \sum_{i=1}^{n} [\vec{\mathbf{H}}^{(1)i} + \vec{\mathbf{H}}^{(2)i} + \vec{\mathbf{H}}^{(3)i}] \quad (20)$$

where

$$\vec{\mathbf{H}}^{(1)i} = \{[\vec{\mathbf{h}}_T^{\,e\mathrm{IVm}i} + h_z^{e\mathrm{IVm}i}\hat{\mathbf{u}}_z | \vec{\mathbf{h}}_T^{\,m\mathrm{IVm}i}] \operatorname{diag}[\sqrt{Y_{p,q}^{e,m\mathrm{IVm}i}} \exp[-jk_{zp,q}^{e,m\mathrm{IVm}i}(z - c_{i-1})]]\mathbf{T}_{\mathrm{A}i-1}^{(1)}$$

$$- [\vec{\mathbf{h}}_T^{\,e\mathrm{IVm}i} - h_z^{e\mathrm{IVm}i}\,\hat{\mathbf{u}}_z | \vec{\mathbf{h}}_T^{\,m\mathrm{IVm}i}] \operatorname{diag}[\sqrt{Y_{p,q}^{e,m\mathrm{IVm}i}} \exp[jk_{zp,q}^{e,m\mathrm{IVm}i}(z - c_{i-1})]]\mathbf{T}_{\mathrm{B}i-1}^{(1)}\}\mathbf{M}^{\mathrm{I}}[\mathbf{A}^{\mathrm{I}} + \mathbf{B}^{\mathrm{I}}]$$

$$\vec{\mathbf{H}}^{(2)i} = \{[\vec{\mathbf{h}}_T^{\,e\mathrm{IVm}i} + h_z^{e\mathrm{IVm}i}\hat{\mathbf{u}}_z | \vec{\mathbf{h}}_T^{\,m\mathrm{IVm}i}] \operatorname{diag}[\sqrt{Y_{p,q}^{e,m\mathrm{IVm}i}} \exp[-jk_{zp,q}^{e,m\mathrm{IVm}i}(z - c_i)]]\mathbf{T}_{\mathrm{A}i}^{(2)}$$

$$- [\vec{\mathbf{h}}_T^{\,e\mathrm{IVm}i} - h_z^{e\mathrm{IVm}i}\,\hat{\mathbf{u}}_z | \vec{\mathbf{h}}_T^{\,m\mathrm{IVm}i}] \operatorname{diag}[\sqrt{Y_{p,q}^{e,m\mathrm{IVm}i}} \exp[jk_{zp,q}^{e,m\mathrm{IVm}i}(z - c_i)]]\mathbf{T}_{\mathrm{B}i}^{(2)}\}\mathbf{M}^{\mathrm{II}}[\mathbf{A}^{\mathrm{II}} + \mathbf{B}^{\mathrm{II}}]$$

$$\vec{\mathbf{H}}^{(3)i} = \{[\vec{\mathbf{h}}_T^{\,e\mathrm{IVb}i} + h_y^{e\mathrm{IVb}i}\hat{\mathbf{u}}_y | \vec{\mathbf{h}}_T^{\,m\mathrm{IVb}i}] \operatorname{diag}[\sqrt{Y_{p,q}^{e,m\mathrm{IVb}i}} \exp[-jk_{yp,q}^{e,m\mathrm{IVb}i}(y - b_j)]]\mathbf{T}_{\mathrm{B}j}^{(3)}$$

$$- [\overrightarrow{\mathbf{h}}_T^{e\mathrm{IV}bi} - h_y^{e\mathrm{IV}bi}\,\hat{\mathbf{u}}_y|\overrightarrow{\mathbf{h}}_T^{m\mathrm{IV}bi}]\ \mathrm{diag}\,[\sqrt{Y_{p,q}^{e,m\mathrm{IV}bi}}\ \exp[jk_{yp,q}^{e,m\mathrm{IV}bi}\,(y - b_j)]]\mathbf{T}_{\mathrm{A}j}^{(3)}\}\mathbf{M}^{\mathrm{III}}[\mathbf{A}^{\mathrm{III}} + \mathbf{B}^{\mathrm{III}}] \quad (21)$$

and

$$\mathbf{M}^{\mathrm{I}} = [\mathbf{I} - \Gamma^{\mathrm{I}}]^{-1},\ \mathbf{M}^{\mathrm{II}} = [\mathbf{I} - \Gamma^{\mathrm{II}}]^{-1},\ \mathbf{M}^{\mathrm{III}} = [\mathbf{I} - \Gamma^{\mathrm{III}}]^{-1} \quad (22)$$

Matching the magnetic fields at the interfaces between waveguides I, II and III with the discontinuity-distorted resonator region will relate the amplitude coefficients to yield the desired generalized scattering matrix of the junction. The continuity equations at $z = 0$, c_n and at $y = b_n$ for the tangential magnetic fields are

$$\overrightarrow{\mathbf{H}}_{x,y}^{\mathrm{I}} = \overrightarrow{\mathbf{H}}_{x,y}^{\mathrm{IV}} = \sum_{i=1}^{n} [\overrightarrow{\mathbf{H}}_{x,y}^{(1)i} + \overrightarrow{\mathbf{H}}_{x,y}^{(2)i} + \overrightarrow{\mathbf{H}}_{x,y}^{(3)i}] = \overrightarrow{\mathbf{H}}_{x,y}^{(1)1} + \overrightarrow{\mathbf{H}}_{x,y}^{(2)1} + \sum_{i=1}^{n} \overrightarrow{\mathbf{H}}_{x,y}^{(3)i} \text{ at } z = 0 \quad (23)$$

$$\overrightarrow{\mathbf{H}}_{x,y}^{\mathrm{II}} = \overrightarrow{\mathbf{H}}_{x,y}^{\mathrm{IV}} = \overrightarrow{\mathbf{H}}_{x,y}^{(1)n} + \overrightarrow{\mathbf{H}}_{x,y}^{(2)n} + \sum_{i=1}^{n} \overrightarrow{\mathbf{H}}_{x,y}^{(3)i} \text{ at } z = c_n \quad (24)$$

$$\overrightarrow{\mathbf{H}}_{x,z}^{\mathrm{III}} = \overrightarrow{\mathbf{H}}_{x,z}^{\mathrm{IV}} = \sum_{i=1}^{n} \overrightarrow{\mathbf{H}}_{x,z}^{(1)i} + \sum_{i=1}^{n} \overrightarrow{\mathbf{H}}_{x,z}^{(2)i} + \overrightarrow{\mathbf{H}}_{x,z}^{(3)1} \text{ at } y = b_n \quad (25)$$

which, when integrated over the respective interface areas and employing the principles of orthogonality, result in the matrix equation

$$\begin{bmatrix} -\mathbf{I} - [\mathbf{I} - \Gamma^{\mathrm{I}}]\,\mathbf{M}^{\mathrm{I}} & -[\mathbf{U}_{\mathrm{A}}^{(2)}\mathbf{T}_{\mathrm{A}0}^{(2)} - \mathbf{U}_{\mathrm{B}}^{(2)}\mathbf{T}_{\mathrm{B}0}^{(2)}]\,\mathbf{M}^{\mathrm{II}} & -\mathbf{V}^{\mathrm{I}-(3)}\mathbf{M}^{\mathrm{III}} \\ -[\mathbf{U}_{\mathrm{A}}^{(1)}\mathbf{T}_{\mathrm{A}n-1}^{(1)} - \mathbf{U}_{\mathrm{B}}^{(1)}\mathbf{T}_{\mathrm{B}n-1}^{(1)}]\,\mathbf{M}^{\mathrm{I}} & \mathbf{I} + [\mathbf{I} - \Gamma^{\mathrm{II}}]\,\mathbf{M}^{\mathrm{II}} & -\mathbf{V}^{\mathrm{II}-(2)}\mathbf{M}^{\mathrm{III}} \\ -\mathbf{V}^{\mathrm{III}-(1)}\mathbf{M}^{\mathrm{I}} & -\mathbf{V}^{\mathrm{III}-(2)}\mathbf{M}^{\mathrm{II}} & \mathbf{I} + [\mathbf{I} - \Gamma^{\mathrm{III}}]\mathbf{M}^{\mathrm{III}} \end{bmatrix} \begin{bmatrix} \mathbf{B}^{\mathrm{I}} \\ \mathbf{B}^{\mathrm{II}} \\ \mathbf{B}^{\mathrm{III}} \end{bmatrix}$$

$$= \begin{bmatrix} -\mathbf{I} + [\mathbf{I} - \Gamma^{\mathrm{I}}]\,\mathbf{M}^{\mathrm{I}} & [\mathbf{U}_{\mathrm{A}}^{(2)}\mathbf{T}_{\mathrm{A}0}^{(2)} - \mathbf{U}_{\mathrm{B}}^{(2)}\mathbf{T}_{\mathrm{B}0}^{(2)}]\,\mathbf{M}^{\mathrm{II}} & \mathbf{V}^{\mathrm{I}-(3)}\mathbf{M}^{\mathrm{III}} \\ [\mathbf{U}_{\mathrm{A}}^{(1)}\mathbf{T}_{\mathrm{A}n-1}^{(1)} - \mathbf{U}_{\mathrm{B}}^{(1)}\mathbf{T}_{\mathrm{B}n-1}^{(1)}]\,\mathbf{M}^{\mathrm{I}} & \mathbf{I} - [\mathbf{I} - \Gamma^{\mathrm{II}}]\,\mathbf{M}^{\mathrm{II}} & \mathbf{V}^{\mathrm{II}-(2)}\mathbf{M}^{\mathrm{III}} \\ \mathbf{V}^{\mathrm{III}-(1)}\mathbf{M}^{\mathrm{I}} & \mathbf{V}^{\mathrm{III}-(2)}\mathbf{M}^{\mathrm{II}} & \mathbf{I} - [\mathbf{I} - \Gamma^{\mathrm{III}}]\mathbf{M}^{\mathrm{III}} \end{bmatrix} \begin{bmatrix} \mathbf{A}^{\mathrm{I}} \\ \mathbf{A}^{\mathrm{II}} \\ \mathbf{A}^{\mathrm{III}} \end{bmatrix} \quad (26)$$

from which the generalized scattering matrix of the discontinuity-distorted junction

$$\begin{bmatrix} \mathbf{B}^{\mathrm{I}} \\ \mathbf{B}^{\mathrm{II}} \\ \mathbf{B}^{\mathrm{III}} \end{bmatrix} = \begin{bmatrix} \mathbf{S}_{11}\ \mathbf{S}_{12}\ \mathbf{S}_{13} \\ \mathbf{S}_{21}\ \mathbf{S}_{22}\ \mathbf{S}_{23} \\ \mathbf{S}_{31}\ \mathbf{S}_{32}\ \mathbf{S}_{33} \end{bmatrix} \begin{bmatrix} \mathbf{A}^{\mathrm{I}} \\ \mathbf{A}^{\mathrm{II}} \\ \mathbf{A}^{\mathrm{III}} \end{bmatrix} \quad (27)$$

can be derived as demonstrated in Appendix I. The remaining abbreviations used in (26) are detailed in Appendix II.

Now it is possible to address the two points deferred earlier in this Section. Firstly, the formulation can, indeed, accommodate discontinuities with variations along the *x*-axis. The incorporation of such a discontinuity is accomplished by determining its generalized scattering matrix and following the above formulation — now, however, with the possibility of a subregion in IV being further subdivided, thus producing an internal summation of its own. Secondly, with regard to the condition requiring that adjacent subregions to connecting waveguides have the same cross-sectional dimensions: in configurations where discontinuities appear in an aperture, the problem may be addressed by the insertion of the required subregion and the mathematical reduction of its length to zero. Consequently, other circuit components can be connected to the multiport junction at zero length without any restrictions on the mode spectra at either side of the aperture. Since all fundamental and higher-order modes are appropriately related to each other, the concept of the generalized scattering matrix is fully preserved.

3. RESULTS

Three configurations are selected for the verification and demonstration of this theory. They are the rectangular-waveguide corner, the *E*-plane T-junction power divider and the rectangular-waveguide orthomode transducer. Although it is not the intention of this appraoch to be used for modelling mitred discontinuities, reference data for the type of discontinuities investigated in this paper are difficult to find as they have not been exploited yet for circuit design, simply because of the lack of sufficient CAD tools. Therefore, we will compare our theory with some mitred structures.

Figure 3 shows a comparison for the example of a mitred waveguide corner.[16] The structure is used in dual-mode operation with square waveguide cross-sections. It is analysed by neglecting region II and solution IV(2) in the theory to form a discontinuity-distorted corner junction. Since a full-mode spectrum is used, both polarizations (modes TE_{10} and TE_{01}) are obtained simultaneously as elements of the generalized scattering matrix. Figure 3(a) shows the results for the vertical (TE_{10}-mode) polarization. The convergence analysis — with respect to the number of steps to approximate the mitre — indicates that nine to 12 steps are a good mitre approximation for this polarization. A similar analysis regarding the number of modes (not shown) produces sufficient convergence behaviour at 20–25 modes. Good agreement with the results of Reference 16 is observed in Figure 3(a), except for the resonance effect around 9 GHz. Unfortunately, the spacing of measured data in frequency is relatively wide in Reference 16 so that the resonance cannot be confirmed exactly. However, this effect is well known in square-waveguide applications, e.g. Reference 6, where it appears below the TE_{11}-mode cutoff frequency. In this case, TE_{11}-mode cutoff occurs at 9·27GHz as indicated by the small dips in the computed results at that frequency.

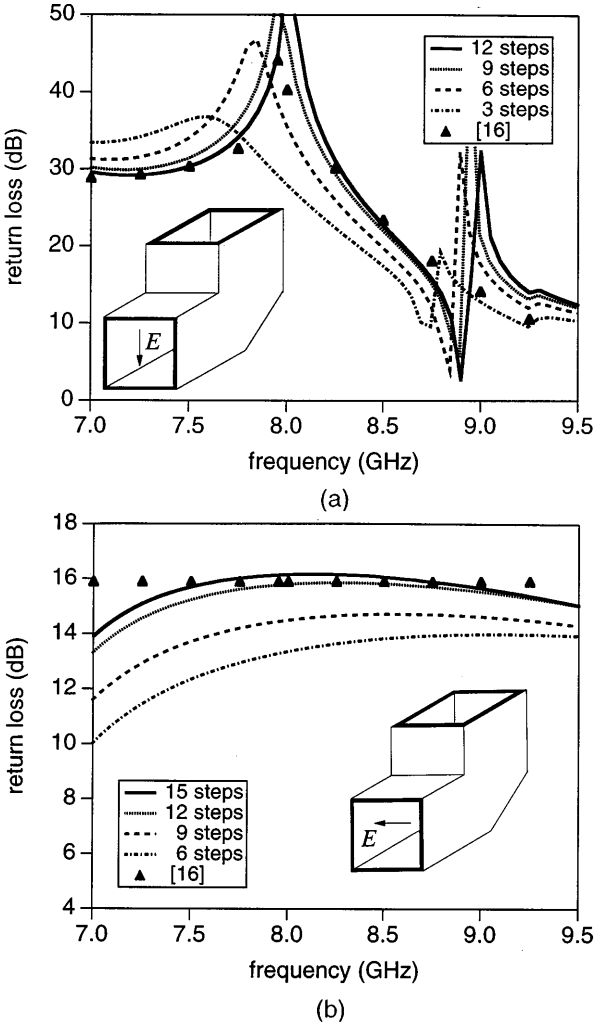

Figure 3. Input return loss of mitred dual-mode square waveguide corner. Dimensions: $a = b = c = d = 22{\cdot}86$ mm; 45° mitre[16] approximated by constant stepping with $c_1 = b_{n-1} = 5{\cdot}08$ mm; (a) vertical polarization; (b) horizontal polarization

The results for the horizontal (TE_{01}-mode) polarization are shown in Figure 3(b). Since the electric field vector is now tangential to the mitre, a stepped approximation must show a more pronounced frequency dependence than the straight mitre. As a consequence, and in order to compare our computations with the mitred results of Reference 16, the number of steps in our model need to be increased (results for up to 15 steps are shown in Figure 3(b)). Moreover, as the number of steps is increased, the individual staircase sections become shorter, thus requiring more higher-order modes to be included (up to 35 modes are used here). Considering these points under the restriction of finite computer resources, it is obvious that good agreement with the straight mitre of Reference 16 — for horizontal polarization — can only be achieved over a limited frequency range. With 15 steps and 35 modes, agreement is good between 7·5 and 9 GHz. Note that this horizontal (TE_{01}-mode) polarization couples only with higher-order TE_{0n}-mode field configurations. Therefore, the response is not affected by the TE_{11} mode.

180 degree *E*-plane bends are frequently used in beam-forming networks. For such a structure, a comparison between our results and those of a finite-element analysis is presented in Figure 4. In our approach, the generalized modal scattering matrices of the two discontinuity-distorted corners are calculated and properly cascaded. Owing to the interaction of modes between the two 90 degree corners, it is important to consider the full-mode spectrum in the cascading process, as is done with this theory. Very good agreement is achieved with a five-step approximation of the mitres. Note that discrepancies are observed mainly beyond the 30dB level. Therefore, it is idle to argue in favour of the accuracy of either one of the two numerical techniques, finite element or mode matching.

Figures 5 show the performances related to the T-junction power divider. For a first verification of the theory, the single-step T-junction power divider of Reference 1 has been recalculated with this method. By using the technique of inserting a subregion and reducing its mathematical length to zero (as explained in the theory section), the single *E*-plane step is placed directly in the aperture (inset Figure 5(a)). Good agreement within the readability of the data in Reference 1 is obtained for both return loss (Figure 5(a)) and insertion loss (Figure 5(b)).

Several experiments have been conducted with additional steps in the junction region. Owing to the multiple-step approach and its effective size reduction of the junction area, the return loss no longer exhibits a relatively narrow peak but broadens over the frequency range of interest. This is demonstrated by a five-step design in Figure 5(a) (solid line). Consequently, a minimum return-loss performance of 22 dB can be provided (compared to 15·5 dB in Reference 1) over the entire frequency range 10–16 GHz. Due to its improved return loss, the component with five steps in the junction exhibits slightly better power division (solid lines in Figure 5(b)) than the standard junction design. A power division within +0·9 and –0·6 dB is obtained over the entire frequency range of Figure 5. (The respective values in Reference 1 are +1·3 and –0·8 dB.)

At the example of a rectangular-waveguide orthomode transducer proposed in Reference 7 and sketched in Figure 6(a), Figure 6(b) compares the measurements of Reference 7 with the results of this technique. Note that this component requires the computation of the full generalized

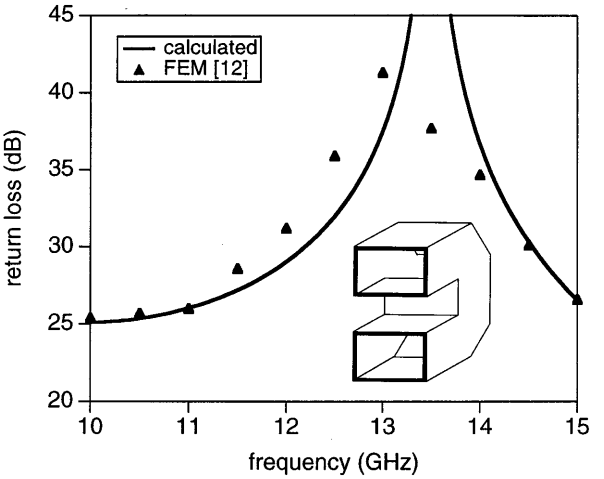

Figure 4. Comparison of this method with finite-element method (FEM) at a 180 degree *E*-plane bend.[12] Dimension: $a = d = 19{\cdot}05$ mm, $b = 5{\cdot}08$ mm, $c = 4{\cdot}826$ mm, vertical separation between rectangular guides = 6·096 mm; 45° mitres[12] approximated by five steps with $c_1 = b_{n-1} = 0{\cdot}659$ mm

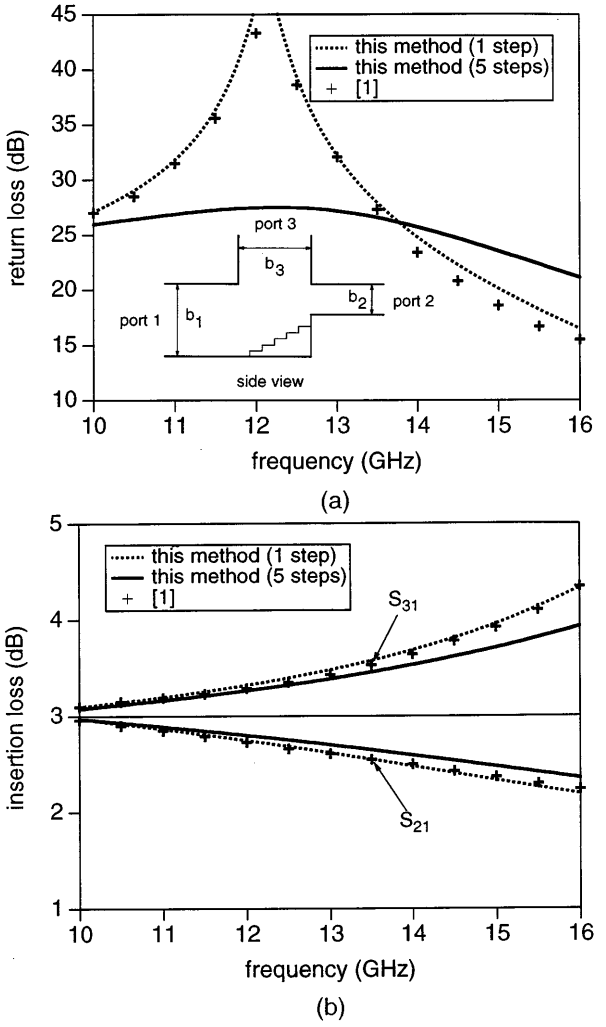

Figure 5. Performance of *E*-plane T-junction power divider. Dimensions: $a = d = 2b_1 = 15{\cdot}799$ mm, $b_2 = 4{\cdot}41$ mm, $b_3 = 4{\cdot}38$ mm.[1] Undistorted junction: this method (dashed lines); data from Reference 1 (+++). Stepped junction: this method (solid line); 18·5° mitre approximated by five steps with $c_1 = 0$ and $b_{n-1} = b_1 - b_2$; (a) input return loss; (b) insertion loss

scattering matrix of the discontinuity-distorted junction region as the matching iris in the branching waveguide is connected to the junction at zero distance. Therefore, virtually all higher-order modes interact. The analysis of this component with the so-called three-plane mode-matching technique, or modifications thereof, would be highly questionable due to its restriction to the fundamental-mode scattering matrix of the discontinuity-distorted junction. Since our technique includes such higher-order mode effects, good agreement with measurements in Reference 7 can be observed (Figure 6(b)). The discrepancies are attributed to the fact that the linear taper in Reference 7 has been approximated by a 25-step staircase function in this theory.

With 25 modes in each of the subregions, the computation of this structure requires 20 min of CPU time per frequency point on an IBM RISC 6000/530 workstation. The maximum time required for other structures might be estimated from this value as the CPU time depends — as a rough first-order approximation — linearily on the number of steps in the junction region and increases with the third power (corresponding to matrix inversion) with the number of modes.

4. CONCLUSION

A new generalized scattering matrix formulation for discontinuity-distorted waveguide multiport junctions is presented. Since the discontinuities in the junction region are rigorously taken into account, with their influences transformed to the interfaces with the connected rectangular waveguides, the *generalized* scattering matrix — as opposed to hitherto known fundamental-mode

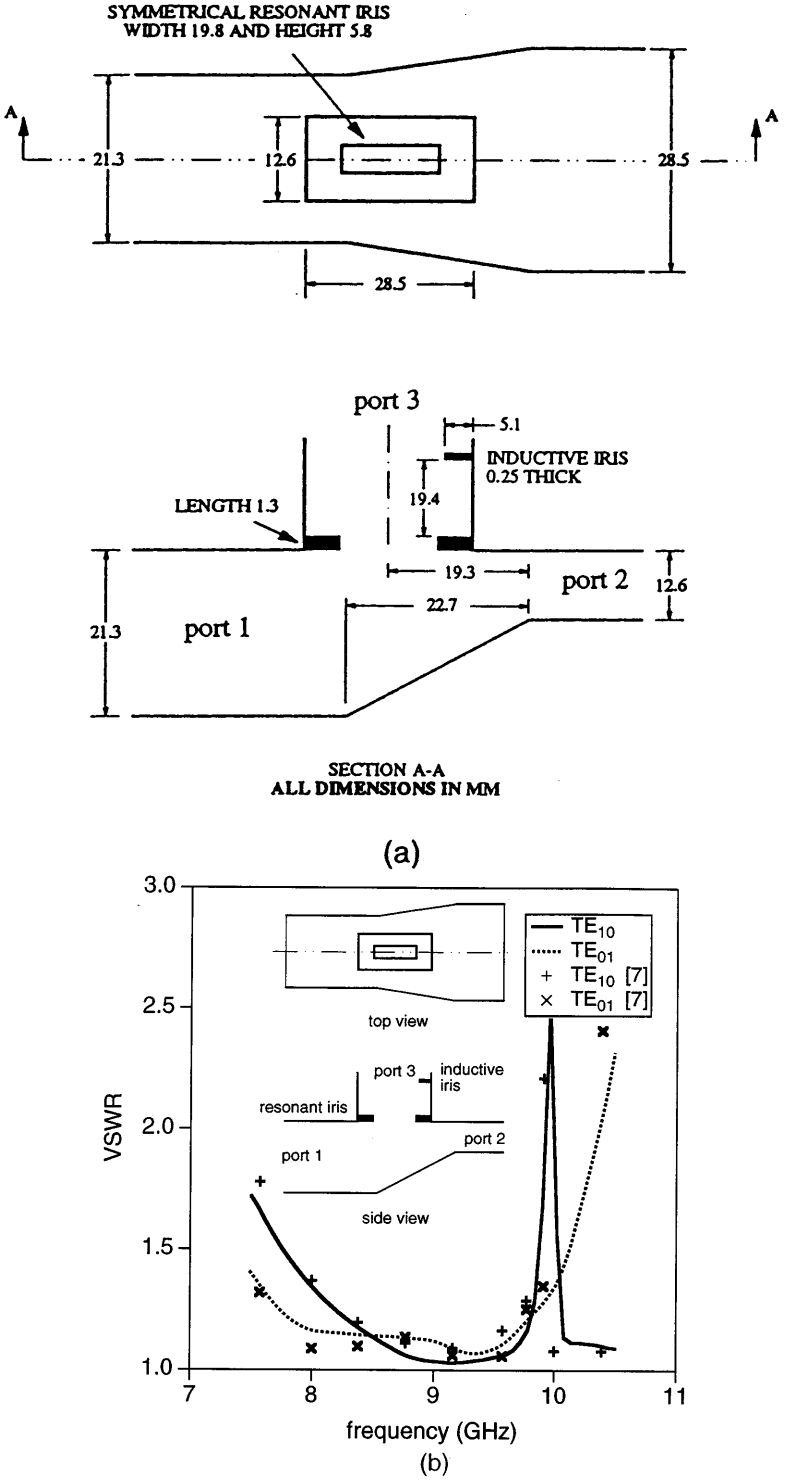

Figure 6. Rectangular-waveguide orthomode transducer according to Reference 7. Dimensions (a) and VSWR comparison (b). This method (solid lines), measurement (+++) of Reference 7. Note that the continuous transition in Reference 7 is approximated by a 25-step approach

parameters — of such structures can be calculated. At the examples of waveguide corners, a T-junction power divider and an orthomode transducer, good agreement with other techniques and measurements available from the literature is demonstrated.

APPENDIX I. From (26) to (27)

Of course, (26) can be solved by simple matrix inversion. However, computation efficiency can best be served by a submatrix-based approach. Therefore, (26) is rewritten as

$$\begin{bmatrix} -\mathbf{I}-\mathbf{M} & -\mathbf{M}_2 & -\mathbf{M}_3 \\ -\mathbf{M}_4 & \mathbf{I}+\mathbf{M}_5 & -\mathbf{M}_6 \\ -\mathbf{M}_7 & -\mathbf{M}_8 & \mathbf{I}+\mathbf{M}_9 \end{bmatrix} \begin{bmatrix} \mathbf{B}^{\mathrm{I}} \\ \mathbf{B}^{\mathrm{II}} \\ \mathbf{B}^{\mathrm{III}} \end{bmatrix} = \begin{bmatrix} -\mathbf{I}+\mathbf{M}_1 & \mathbf{M}_2 & \mathbf{M}_3 \\ \mathbf{M}_4 & \mathbf{I}-\mathbf{M}_5 & \mathbf{M}_6 \\ \mathbf{M}_7 & \mathbf{M}_8 & \mathbf{I}-\mathbf{M}_9 \end{bmatrix} \begin{bmatrix} \mathbf{A}^{\mathrm{I}} \\ \mathbf{A}^{\mathrm{II}} \\ \mathbf{A}^{\mathrm{III}} \end{bmatrix} \tag{28}$$

and the variable **B** is partially separated by

$$\begin{aligned} \mathbf{B}^{\mathrm{I}} &= \mathbf{N}_1\mathbf{N}_2\mathbf{B}^{\mathrm{III}} + \mathbf{N}_1\mathbf{N}_2\mathbf{A}^{\mathrm{I}} + \mathbf{N}_1\mathbf{N}_4\mathbf{A}^{\mathrm{II}} + \mathbf{N}_1\mathbf{N}_2\mathbf{A}^{\mathrm{III}} \\ \mathbf{B}^{\mathrm{II}} &= \mathbf{N}_5\mathbf{N}_6\mathbf{B}^{\mathrm{III}} + \mathbf{N}_5\mathbf{N}_7\mathbf{A}^{\mathrm{I}} + \mathbf{N}_5\mathbf{N}_8\mathbf{A}^{\mathrm{II}} + \mathbf{N}_5\mathbf{N}_6\mathbf{A}^{\mathrm{III}} \end{aligned} \tag{29}$$

with

$$\begin{aligned} \mathbf{N}_1 &= [-(\mathbf{I}+\mathbf{M}_1) + \mathbf{M}_2\,(\mathbf{I}+\mathbf{M}_5)^{-1}\,\mathbf{M}_4]^{-1} & \mathbf{N}_5 &= [-(\mathbf{I}+\mathbf{M}_5) + \mathbf{M}_4\,(\mathbf{I}+\mathbf{M}_1)^{-1}\mathbf{M}_2]^{-1} \\ \mathbf{N}_2 &= \mathbf{M}_3 + \mathbf{M}_2\,(\mathbf{I}+\mathbf{M}_5)^{-1}\,\mathbf{M}_6 & \mathbf{N}_6 &= \mathbf{M}_6 + \mathbf{M}_4\,(\mathbf{I}+\mathbf{M}_1)^{-1}\,\mathbf{M}_3 \\ \mathbf{N}_3 &= -\,(\mathbf{I}-\mathbf{M}_1) + \mathbf{M}_2\,(\mathbf{I}+\mathbf{M}_5)^{-1}\,\mathbf{M}_4 & \mathbf{N}_7 &= \mathbf{M}_4\,[\mathbf{I}+(\mathbf{I}+\mathbf{M}_1)^{-1}\,(\mathbf{I}-\mathbf{M}_1)] \\ \mathbf{N}_4 &= \mathbf{M}_2\,[\mathbf{I}+(\mathbf{I}+\mathbf{M}_5)^{-1}\,(\mathbf{I}-\mathbf{M}_5)] & \mathbf{N}_8 &= (\mathbf{I}-\mathbf{M}_5) - \mathbf{M}_4\,(\mathbf{I}+\mathbf{M}_1)^{-1}\,\mathbf{M}_2 \end{aligned} \tag{30}$$

Hence,

$$\mathbf{B}^{\mathrm{III}} = \mathbf{S}_{31}\mathbf{A}^{\mathrm{I}} + \mathbf{S}_{32}\mathbf{A}^{\mathrm{II}} + \mathbf{S}_{33}\mathbf{A}^{\mathrm{III}} \tag{31}$$

where

$$\begin{aligned} \mathbf{S}_{31} &= \mathbf{Y}[\mathbf{M}_7\,(\mathbf{I}+\mathbf{N}_1\mathbf{N}_3) + \mathbf{M}_8\mathbf{N}_5\mathbf{N}_7] \\ \mathbf{S}_{32} &= \mathbf{Y}[\mathbf{M}_8 + \mathbf{M}_7\mathbf{N}_1\mathbf{N}_4 + \mathbf{M}_8\mathbf{N}_5\mathbf{N}_8] \\ \mathbf{S}_{33} &= \mathbf{Y}\,[(\mathbf{I}+\mathbf{M}_9) + \mathbf{M}_7\mathbf{N}_1\mathbf{N}_2 + \mathbf{M}_8\mathbf{N}_5\mathbf{N}_6] \end{aligned} \tag{32}$$

and

$$\mathbf{Y} = [(\mathbf{I}+\mathbf{M}_9) - \mathbf{M}_7\mathbf{N}_1\mathbf{N}_2 - \mathbf{M}_8\mathbf{N}_5\mathbf{N}_6]^{-1} \tag{33}$$

This now allows the expression of the complete generalized scattering matrix as

$$\begin{aligned} \mathbf{B}^{\mathrm{I}} &= \mathbf{S}_{11}\mathbf{A}^{\mathrm{I}} + \mathbf{S}_{12}\mathbf{A}^{\mathrm{II}} + \mathbf{S}_{13}\mathbf{A}^{\mathrm{III}} \\ \mathbf{B}^{\mathrm{II}} &= \mathbf{S}_{21}\mathbf{A}^{\mathrm{I}} + \mathbf{S}_{22}\mathbf{A}^{\mathrm{II}} + \mathbf{S}_{23}\mathbf{A}^{\mathrm{III}} \end{aligned} \tag{34}$$

where

$$\begin{aligned} \mathbf{S}_{11} &= \mathbf{N}_1[\mathbf{N}_2\mathbf{S}_{31} + \mathbf{N}_3] & \mathbf{S}_{21} &= \mathbf{N}_5[\mathbf{N}_6\mathbf{S}_{31} + \mathbf{N}_7] \\ \mathbf{S}_{12} &= \mathbf{N}_1[\mathbf{N}_2\mathbf{S}_{32} + \mathbf{N}_4] & \mathbf{S}_{22} &= \mathbf{N}_5[\mathbf{N}_6\mathbf{S}_{32} + \mathbf{N}_8] \\ \mathbf{S}_{13} &= \mathbf{N}_1\mathbf{N}_2[\mathbf{S}_{33} + \mathbf{I}] & \mathbf{S}_{23} &= \mathbf{N}_5\mathbf{N}_6\,[\mathbf{S}_{33} + \mathbf{I}] \end{aligned} \tag{35}$$

Five matrix inversions of one-third the size of the original matrix (26) are required by this algorithm, which reduces the CPU time to 1/5·4 of that of a single inversion in (26).

APPENDIX II. Abbreviations in (26)

In (26), matrices **U** are given by

$$\begin{aligned}
\mathbf{U}_{\mathrm{A}}^{(1)} &= \mathrm{diag}\ \{\exp\ [-jk_{zp,q}^{e,m\mathrm{IVmn}}\ (c_n - c_{n-1})]\}\\
\mathbf{U}_{\mathrm{B}}^{(1)} &= \mathrm{diag}\ \{\exp\ [jk_{zp,q}^{e,m\mathrm{IVmn}}\ (c_n - c_{n-1})]\}\\
\mathbf{U}_{\mathrm{A}}^{(2)} &= \mathrm{diag}\ \{\exp\ [jk_{zp,q}^{e,m\mathrm{IVm1}}\ c_1]\}\\
\mathbf{U}_{\mathrm{B}}^{(2)} &= \mathrm{diag}\ \{\exp\ [-jk_{zp,q}^{e,m\mathrm{IVm1}}\ c_1]\}
\end{aligned} \tag{36}$$

and matrices **V** contain the coupling matrices for the junction:

$$\begin{aligned}
\mathbf{V}^{\mathrm{I}-(3)} &= \sum_{i=1}^{n}\ [{}^{+}\mathbf{K}^{\mathrm{I}-(3)i}\mathbf{T}_{\mathrm{B}n-i+1}^{(3)} - {}^{-}\mathbf{K}^{\mathrm{I}-(3)i}\mathbf{T}_{\mathrm{A}n-i+1}^{(3)}]\\
\mathbf{V}^{\mathrm{II}-(3)} &= \sum_{i=1}^{n}\ [{}^{+}\mathbf{K}^{\mathrm{II}-(3)i}\mathbf{T}_{\mathrm{B}n-i+1}^{(3)} - {}^{-}\mathbf{K}^{\mathrm{II}-(3)i}\mathbf{T}_{\mathrm{A}n-i+1}^{(3)}]\\
\mathbf{V}^{\mathrm{III}-(1)} &= \sum_{i=1}^{n}\ [{}^{+}\mathbf{K}^{\mathrm{III}-(1)i}\mathbf{T}_{\mathrm{A}i-1}^{(1)} - {}^{-}\mathbf{K}^{\mathrm{III}-(1)i}\mathbf{T}_{\mathrm{B}i-1}^{(1)}]\\
\mathbf{V}^{\mathrm{III}-(2)} &= \sum_{i=1}^{n}\ [{}^{+}\mathbf{K}^{\mathrm{III}-(2)i}\mathbf{T}_{\mathrm{A}i}^{(2)} - {}^{-}\mathbf{K}^{\mathrm{III}-(2)i}\mathbf{T}_{\mathrm{B}i}^{(2)}]
\end{aligned} \tag{37}$$

For $\vartheta = \mathrm{I}, \mathrm{II}$, these coupling matrices are of the form

$${}^{\pm}\mathbf{K}^{\vartheta-(3)} = \begin{bmatrix} {}^{\pm}\mathbf{K}_{11}^{\vartheta-(3)} & {}^{\pm}\mathbf{K}_{12}^{\vartheta-(3)} \\ {}^{\pm}\mathbf{K}_{21}^{\vartheta-(3)} & {}^{\pm}\mathbf{K}_{22}^{\vartheta-(3)} \end{bmatrix} \tag{38}$$

where

$$\begin{aligned}
{}^{\pm}\mathbf{K}_{11pq}^{\vartheta-(3)i} &= \sqrt{Z_p^{ej}}\ \sqrt{Y_q^{e\mathrm{IVb}i}} \int_{\Delta S_j} \vec{\mathbf{h}}_{Tp}^{\,ej} \cdot (\vec{\mathbf{h}}_{Tq}^{\,e\mathrm{IVb}i} \pm h_{yq}^{e\mathrm{IVb}i}\ \hat{\mathbf{u}}_y)\ \exp\ [\mp jk_{yq}^{e\mathrm{IVb}i}\ (y - b_{(\vartheta)i})]\mathrm{d}S\\
{}^{\pm}\mathbf{K}_{12pq}^{\vartheta-(3)i} &= \sqrt{Z_p^{ej}}\ \sqrt{Y_q^{m\mathrm{IVb}i}} \int_{\Delta S_j} \vec{\mathbf{h}}_{Tp}^{\,ej} \cdot \vec{\mathbf{h}}_{Tq}^{\,m\mathrm{IVb}i}\ \exp\ [\mp jk_{yq}^{m\mathrm{IVb}i}\ (y - b_{(\vartheta)i})]\mathrm{d}S\\
{}^{\pm}\mathbf{K}_{21pq}^{\vartheta-(3)i} &= \sqrt{Z_p^{mj}}\ \sqrt{Y_q^{e\mathrm{IVb}i}} \int_{\Delta S_j} \vec{\mathbf{h}}_{Tp}^{\,mj} \cdot (\vec{\mathbf{h}}_{Tq}^{\,e\mathrm{IVb}i} \pm h_{yq}^{e\mathrm{IVb}i}\ \hat{\mathbf{u}}_y)\ \exp\ [\mp jk_{yq}^{e\mathrm{IVb}i}\ (y - b_{(\vartheta)i})]\mathrm{d}S\\
{}^{\pm}\mathbf{K}_{22pq}^{\vartheta-(3)i} &= \sqrt{Z_p^{mj}}\ \sqrt{Y_q^{m\mathrm{IVb}i}} \int_{\Delta S_j} \vec{\mathbf{h}}_{Tp}^{\,mj} \cdot \vec{\mathbf{h}}_{Tq}^{\,m\mathrm{IVb}i}\ \exp\ [\mp jk_{yq}^{m\mathrm{IVb}i}\ (y - b_{(\vartheta)i})]\mathrm{d}S
\end{aligned} \tag{39}$$

and for $\nu = 1, 2$

$${}^{\pm}\mathbf{K}^{\mathrm{III}-(\nu)} = \begin{bmatrix} {}^{\pm}\mathbf{K}_{11}^{\mathrm{III}-(\nu)} & {}^{\pm}\mathbf{K}_{12}^{\mathrm{III}-(\nu)} \\ {}^{\pm}\mathbf{K}_{21}^{\mathrm{III}-(\nu)} & {}^{\pm}\mathbf{K}_{22}^{\mathrm{III}-(\nu)} \end{bmatrix} \tag{40}$$

where

$${}^{\pm}\mathbf{K}_{11pq}^{\mathrm{III}-(\nu)\mathrm{i}} = \sqrt{Z_p^{e\mathrm{III}}}\ \sqrt{Y_q^{e\mathrm{IVm}i}} \int_{\Delta S^{\mathrm{III}}} \vec{\mathbf{h}}_{Tp}^{\,e\mathrm{III}} \cdot (\vec{\mathbf{h}}_{Tq}^{\,e\mathrm{IVm}i} \pm h_{zq}^{e\mathrm{IVm}i}\ \hat{\mathbf{u}}_z)\ \exp\ [\mp jk_{zq}^{e\mathrm{IVm}i}\ (z - c_{(\nu)i})]\mathrm{d}S$$

$$
\begin{aligned}
{}^{\pm}\mathbf{K}^{\mathrm{III}-(\nu)\mathrm{i}}_{12pq} &= \sqrt{Z^{e\mathrm{III}}_{p}}\,\sqrt{Y^{m\mathrm{IV}mi}_{q}}\int_{\Delta S^{\mathrm{III}}} \vec{\mathbf{h}}^{\,e\mathrm{III}}_{Tp}\cdot\vec{\mathbf{h}}^{\,m\mathrm{IV}mi}_{Tq}\exp\left[\mp jk^{m\mathrm{IV}mi}_{zq}\,(z-c_{(\nu)i})\right]\mathrm{d}S\\
{}^{\pm}\mathbf{K}^{\mathrm{III}-(\nu)\mathrm{i}}_{21pq} &= \sqrt{Z^{m\mathrm{III}}_{p}}\,\sqrt{Y^{e\mathrm{IV}mi}_{q}}\int_{\Delta S^{\mathrm{III}}} \vec{\mathbf{h}}^{\,m\mathrm{III}}_{Tp}\cdot\left(\vec{\mathbf{h}}^{\,e\mathrm{IV}mi}_{Tq}\pm h^{e\mathrm{IV}mi}_{zq}\,\hat{\mathbf{u}}_z\right)\exp\left[\mp jk^{e\mathrm{IV}mi}_{zq}\,(z-c_{(\nu)i})\right]\mathrm{d}S\\
{}^{\pm}\mathbf{K}^{\mathrm{III}-(\nu)\mathrm{i}}_{22pq} &= \sqrt{Z^{m\mathrm{III}}_{p}}\,\sqrt{Y^{m\mathrm{IV}mi}_{q}}\int_{\Delta S^{\mathrm{III}}} \vec{\mathbf{h}}^{\,m\mathrm{III}}_{Tp}\cdot\vec{\mathbf{h}}^{\,m\mathrm{IV}mi}_{Tq}\exp\left[\pm jk^{m\mathrm{IV}mi}_{zq}\,(z-c_{(\nu)i})\right]\mathrm{d}S
\end{aligned}
\tag{41}
$$

and the subscripts on b and c are the co-ordinate shifts for each region. It may be noted that the submatrices in (38) and (40) cover all possible combinations of modal coupling, i.e. TE-to-TE, TE–TM, TM–TE, and TM–TM.

REFERENCES

1. F. Arndt, I. Ahrens, U. Papziner, U. Wiechmann and R. Wilkeit, 'Optimized E-plane T-junction series power dividers', *IEEE Trans. Microw. Theory Tech.*, **MTT-35**, 1052–1059 (1987).
2. T. Sieverding and F. Arndt, 'Field theoretic CAD of open or aperture matched T-junction coupled rectangular waveguide structures', *IEEE Trans. Microw. Theory Tech.*, **40**, 353–362 (1992).
3. X.-P. Liang, K. A. Zaki and A. E. Atia, 'A rigorous three plane mode matching technique for characterizing waveguide T-junctions, and its application in multiplexer design', *IEEE Trans. Microw. Theory Tech.*, **39**, 2138–2147 (1991).
4. H.-W. Yao, A. E. Abdelmonem, J.-F. Liang, X.-P. Liang, K. A. Zaki and A. Martin, 'Wide-band waveguide and ridge waveguide T-junctions for diplexer applications', *IEEE Trans. Microw. Theory Tech.*, **41**, 2166–2173 (1993).
5. F. Alessandri, M. Mongiardo and R. Sorrentino, 'Computer-aided design of beam forming networks for modern satellite antennas', *IEEE Trans. Microw. Theory Tech.*, **40**, 1117–1127 (1992).
6. J. Bornemann and V. A. Labay, 'Ridge waveguide polarizer with finite and stepped-thickness septum', *IEEE Trans. Microw. Theory Tech.*, **43**, 1782–1787 (1995).
7. R. C. Johnson, F. L. Cain and E. N. Bone, 'Dual-mode coupler', *IEEE Trans. Microw. Theory Tech*., **MTT-15**, 651–652 (1967).
8. A.M. Boifot, E. Lier and T-Schaug-Pettersen, 'Simple and broadband orthomode transducers', *IEE Proc. H,* **137**, 396–400 (1990).
9. E. Kühn, 'A mode-matching method for solving field problems in waveguide and resonator circuits', *Arch. Elektr. Übertr.*, **27**, 511–518 (1973).
10. T. Sieverding and F. Arndt, 'Rigorous analysis of the rectangular waveguide six-port cross junction', *IEEE Microw. Guid. Wave Lett.*, **3**, 224–226 (1993).
11. X.-P. Liang, K. A. Zaki and A. E. Atia, 'Characterizing waveguide T-junctions by three plane mode-matching techniques', *1991 IEEE MTT-S Int. Microwave Symp. Dig.*, pp. 849–852.
12. J. Uher, J. Bornemann and U. Rosenberg, *Waveguide Components for Antenna Feed Systems. Theory and CAD*, Artech House Inc., Norwood 1993.
13. A. E. Abdelmonem and K. A. Zaki, 'Slit-coupled ridge waveguide T-junctions', *IEEE Microw. Guid. Wave Lett.*, **5**, 40–41 (1995).
14. Z. Ma and E. Yamashita, 'Port reflection coefficient method for solving multi-port microwave network problems', *IEEE Trans. Microw. Theory Tech.*, **43**, 331–337 (1995).
15. F. Alessandri, G. Bartolucci and R. Sorrentino, 'Admittance matrix formulation of waveguide discontinuity problems: Computer-aided design of branch guide directional couplers', *IEEE Trans. Microw. Theory Tech.*, **36**, 349–403 (1988).
16. P. K. Park, R. L. Eisenhart and S. E. Bradshaw, 'Matched dual mode square waveguide corner', *1986 IEEE MTT-S Int. Microwave Symp. Dig*., pp. 155–156.
17. R. Beyer and F. Arndt, 'Efficient modal analysis of waveguide filters including the orthogonal mode coupling elements by an MM/FE method', *IEEE Microw. Guid. Wave Lett.*, **5**, 9–11 (1995).
18. F. Alessandri, M. Barba, M. Mongiardo and R. Sorrentino, 'Rigorous and efficient analysis of hybrid T-junctions', *1993 IEEE MTT-S Int. Microwave Symp. Dig*., pp. 1447–1450.
19. F. Alessandri, M. Mongiardo and R. Sorrentino, 'Rigorous mode matching analysis of mitered E-plane bends in rectangular waveguide', *IEEE Microw. Guid. Wave Lett.*, **4**, 408–410 (1994).
20. F. Alessandri, M. Dionigi and R. Sorrentino, 'Rigorous analysis of compensated E-plane junctions in rectangular waveguide', *1995 IEEE MTT-S Int. Microwave Symp. Dig*., pp. 987–990.

Authors' biographies:

Vladimir A. Labay was born in Winnipeg, Manitoba, Canada on 11 May 1965. He earned the Bachelor of Science degree in engineering and the Master of Science degree at the University of Manitoba in 1987 and 1990, respectively, and a Doctor of Philosophy (Ph.D) degree in the Department of Electrical Engineering at the University of Victoria, Victoria, British Columbia in 1995. His current research interests include numerical modelling of microwave and millimetre-wave components with emphasis on the characterization of arbitrarily shaped discontinuities within rectangular waveguides.

Jens Bornemann was born in Hamburg, Germany on 26 May 1952. He received the Dipl.-Ing and the Dr.-Ing. degrees, both in electrical engineering, from the University of Bremen, Germany in 1980 and 1984, respectively. From 1980 to 1983, he was a Research and Teaching Assistant in the Microwave Department at the University of Bremen, where he worked on quasi-planar waveguide configurations and computer-aided *E*-plane filter design. In 1985, after a two year period as a consulting engineer, he joined the University of Bremen again and was employed at the level of Assistant Professor. Since April 1988, he has been with the University of Victoria, Victoria, B.C., Canada, where he is currently a Professor in the Department of Electrical and Computer Engineering. His research problems include microwave/millimetre-wave components and systems design, and problems of electromagnetic field theory in integrated circuits and radiating structures. He is a coauthor of *Waveguide Components for Antenna Feed Systems. Theory and Design* (Artech House, 1993) and has authored/coauthored more than 100 technical papers. He is a Registered Professional Engineer in the Province of British Columbia, Canada, and has been a Fellow of the British Columbia Advanced Systems Institute, 1992–1995. Dr. Bornemann was one of the recipients of the A. F. Bulgin Premium of the Institution of Electronic and Radio Engineers in 1983. He is a Senior Member of IEEE and serves on the editorial boards of the *IEEE Transactions on Microwave Theory and Techniques* and the *International Journal of Numerical Modelling.*